The Effect of Divalent Ions on the Structure of Bilayers in the Dimyristoylphosphatidylcholine Vesicles

S. A. Kurakin[a, b], *, E. V. Ermakova[b], A. I. Ivankov[b, c, d], S. G. Smerdova[e], and N. Kučerka[b, f], **

[a]*Institute of Physics, Kazan Federal University, Kazan, 420008 Russia*
[b]*Frank Laboratory of Neutron Physics, Joint Institute for Nuclear Research, Dubna, 141980 Russia*
[c]*Moscow Institute of Physics and Technology, Dolgoprudnyi, 141701 Russia*
[d]*Institute for Safety Problems of Nuclear Power Plants, National Academy of Sciences of Ukraine, Kyiv, 03028 Ukraine*
[e]*Kazan National Research Technological University, Kazan, 420015, Russia*
[f]*Department of Physical Chemistry of Drugs, Faculty of Pharmacy, Comenius University in Bratislava, Bratislava, 832 32 Slovakia*
*e-mail: ksa18@list.ru
**e-mail: kucerka@nf.jinr.ru
Received June 9, 2020; revised August 23, 2020; accepted August 25, 2020

Abstract—We have studied changes in the structural parameters of 1,2-dimyristoyl-sn-3-phosphocholine (DMPC) unilamellar vesicles at a concentration series 0–30 mM of divalent metal cations Ca^{2+}, Mg^{2+}, and Co^{2+} by means of small-angle neutron scattering (SANS). The membrane structural parameters (thickness and area per lipid) were obtained at different concentrations of cations in the gel and fluid phases of membrane. Both Ca^{2+} and Mg^{2+} ions at the concentrations of 0–1 mM increase the membrane thickness by 1.9 Å and 2.9 Å in the fluid and gel phase, respectively. In the concentration range of 1–30 mM, either a weak tendency to a thickness decrease of ~ 1 Å is observed, or the thickness does not change at all. In the case of Co^{2+} ions, all changes are extremely weak. We advocate a model of electrostatic interactions for these systems that encompasses the formation of ion bridges between lipid headgroups. Using the Langmuir adsorption isotherm we estimate the fraction of Ca^{2+} ions bound to the DMPC membrane. The developed model is of an interest to the future studies of membrane interactions with various charged peptides, such as those from the amyloid-β family.

Keywords: lipid membranes, metal ions, thermodynamic state, small-angle neutron scattering, membrane thickness, area per lipid

DOI: 10.1134/S1027451021020075

INTRODUCTION

Biological membranes are extremely significant for the vital activity of a cell, since they play an important role in maintaining its autonomy and posses a number of unique properties associated with the transmission of nerve impulses and the transport of substances [1, 2]. Such properties of membranes are largely determined by the presence of ions in cytoplasm and in the environment surrounding the cell. Monovalent and divalent metal ions are contained in relatively high concentrations and play an important role in the regulation of cell polarization and action potentials [3]. Moreover, divalent ions interact more strongly with phospholipids in comparison with monovalent ions [4], which leads to different effects on the membrane structure. For example, this has been demonstrated on model bacterial membranes composed of lipopolysaccharides (LPS) [5]. According to neutron diffraction data, water penetrates into LPS bilayers containing

Ca^{2+} to a lesser extent than into bilayers with Na^+ ions and the head region of the lipids becomes more dehydrated, which leads to the stronger ordering of chains in the membrane with Ca^{2+} ions [5].

Among all ions, divalent cations of alkaline earth metals, such as Ca^{2+} and Mg^{2+}, are indispensable at certain concentrations and directly take part in signal transduction and tissue mineralization [6, 7]. Transition-metal ions (Co^{2+}, Fe^{2+}, and Cu^{2+}) are necessary for hematopoiesis and metabolism, in contrast to heavy metal ions that are toxic to the body (Hg^{2+}, Cd^{2+}, and Pb^{2+}) [8].

It is well known that metal cations interact with the cell membrane by binding to the polar head of phospholipids that form a bilayer [9–11]. This leads to changes in the thickness and structure of the membrane and has an effect on the functions and conformations of various proteins integrated into it [12], while the ions themselves exhibit specific binding fea-

tures characteristic of each particular ion. In the general case, such specific interactions of ions with proteins, polymers, and a bulk solution are more accurately described by the Hofmeister series, the ions in which are arranged in order of their effect on the properties of the solvent and their effect on the various processes that take place in an aqueous medium. In these series, the sequence of ions is determined by their charge, polarizability, size, and hydration. Since the ionic radii are determined by the number of electron shells and the size of the atomic nucleus, ions with the same charge can have completely different Hofmeister effects [3].

Taking into account that changes in the conformations of proteins and phospholipids during their interactions with ions closely correlate with the membrane thickness, it is obvious that the thermodynamic phase of lipid systems, apart from the length of phospholipid tails, also plays an important role in many interactions [13]. Parallel ordering of the phospholipid chains is observed in the gel phase, which leads to an increase in the thickness of the membrane and denser packing, as well as to a decrease in the fluidity of the bilayer. On the contrary, lipid systems in the fluid phase exhibit increased dynamics and disorder associated with less dense packing.

Currently, many experiments are directed at studying the properties of saturated zwitterionic phospholipids. However, structural studies of these phospholipids in their interactions with divalent metal ions, such as Ca^{2+}, Mg^{2+}, and Co^{2+} are insufficiently comprehensive. Therefore, we continue previous studies of the structural parameters of saturated phospholipid membranes, which were developed in [14] using the 1,2-dipalmitoyl-sn-3-phosphocholine (DPPC) system containing Ca^{2+} ions as an example, and concentrate our efforts on the experimental study of DMPC phospholipid vesicles by small-angle neutron scattering (SANS). The SANS curves obtained from samples of DMPC unilamellar vesicles (ULVs), which separately contained Ca^{2+}, Mg^{2+}, and Co^{2+} ions in the concentration range of 0–30 mM and were placed in D_2O to obtain the maximum contrast conditions for neutron scattering, are analyzed over the entire presented range of the scattering vector q using the following two models: the Kratky–Porod approximation and the spherical vesicle model. The following structural parameters of the bilayer were obtained by approximating the experimental data: bilayer thickness d_b and area per lipid A_L corresponding to one DMPC molecule as functions of the concentration of ions in the solution.

SAMPLE PREPARATION

To prepare the samples of DMPC vesicles, dehydrated lipid (Avanti Polar Lipids, Alabama, United States) was added in a concentration of 50 mg/mL to a mixture of chloroform and methanol solvents taken in a volume ratio of 2 : 1. Next, the solvents were evaporated under a flow of argon or nitrogen to create a lipid film at the bottom of the vials. The complete removal of solvent traces was achieved in a vacuum chamber. Salts $CaCl_2 \cdot 2H_2O$, $MgCl_2 \cdot 6H_2O$, and $CoCl_2 \cdot 6H_2O$ (Sigma-Aldrich, Germany) of the studied ions were used to prepare solutions in D_2O (in the ion concentration range of 0–30 mM), which were then used to hydrate the lipids in the vials (1.5 mL). The system was thoroughly mixed in a shaker and subjected to the freeze–thaw cycles (at least 10 times) through the temperature of the main phase transition. After this procedure, the samples showed a slight opalescence typical of large multilamellar lipid vesicles in a solution.

DMPC ULVs were obtained by extruding the solution of multilamellar vesicles. We used two polycarbonate filters with a pore diameter of 1000 Å (Avanti Polar Lipids, Alabama, United States) for the DMPC + Ca^{2+} (Mg^{2+}) systems and one filter with a pore diameter of 500 Å for the DMPC + Co^{2+} system in an Avanti Polar Lipids extruder (Alabama, United States) equipped with two gastight syringes from Hamilton (Reno, Nevada, United States). The extrusion process was performed mechanically an odd number of times (31 passages of the system through the filters) to prevent large vesicles from entering the sample. The multilamellar DMPC vesicles were extruded through filters in the fluid phase of the lipid by heating the extruder with the sample to a temperature of 50°C. After extrusion, the fully hydrated unilamellar vesicles were incubated for 24 h at room temperature to achieve equilibrium in the system. All samples were extruded in advance (1–3 days before the experiment) to avoid the spontaneous formation of multilamellar vesicles. Immediately before measurements, the samples were transferred to 2 mm quartz cuvettes (Hellma, Germany).

Extrusion through smaller filters more reliably leads to a unilamellar structure of the vesicles, though the structure of the bilayer does not change in the case of uncharged lipids [15]. However, the greater curvature of the membrane can lead to a change in the structure of the bilayer in the presence of charges. Nevertheless, the results that we obtained for vesicles extruded through filters with pore diameters of 1000 and 500 Å revealed no effect of the pore size on the membrane thickness, while the use of filters with a smaller pore diameter improved the unilamellarity of the vesicles, as follows from a noticeable decrease in the Bragg peak intensity.

EXPERIMENTAL

The experiment was performed on a YuMO small-angle elastic neutron scattering spectrometer by the time-of-flight method [16]. The IBR-2 pulsed nuclear reactor (Frank Laboratory of Neutron Physics, Joint

Institute for Nuclear Research, Dubna, Russia) served as the source of neutrons [17].

A beam of thermal neutrons with wavelengths from 0.5 to 8 Å in accordance with the Maxwell distribution statistics was focused by a set of two collimators with diameters of 40 and 14 mm. The neutrons scattered at the sample were recorded by two ring detectors located at a distance of 4.5 and 13 m from the samples, which made it possible to cover the range of the scattering vector q from 0.006 to 0.5 Å^{-1}. The vanadium standard was used to calibrate the absolute scattering intensity, and the buffer solution was used to calibrate the background intensity. The temperature of the samples was controlled by a Lauda thermostat with a Pt-100 temperature probe and was set at 20°C and 30°C to study the gel and fluid phases of the DMPC lipid systems, the main phase-transition temperature of which is 24°C. The SANS curves were obtained using the SAS software package [18].

THEORETICAL ANALYSIS

For centrosymmetric particles in a solution, the intensity of scattered neutrons is determined as follows [19]:

$$I(q) = n|F(q)|^2 S(q) + B, \tag{1}$$

where n is the concentration of particles, q is the scattering vector, $|q| = \left(\frac{4\pi}{\lambda}\right)\sin\left(\frac{\theta}{2}\right)$, θ is the scattering angle, B is the background intensity, $F(q)$ is the form factor of the particle, and $S(q)$ is the structure factor that describes the interaction between particles; in our systems (very dilute systems) with phospholipid concentrations of less than 2 wt %, $S(q) = 1$ [20].

The obtained experimental dependences of the intensity $I(q)$ were analytically approximated (fitted) within the following two models of vesicles: the Kratky–Porod model and the spherical model. In the Kratky–Porod approximation, the intensity can be expressed as follows [21]:

$$I(q) = \frac{A}{q^2} e^{-q^2 R_t^2} + B, \quad R_t q < 1, \tag{2}$$

where A is a constant value that depends on the concentration of vesicles in the system and their volume fraction in a solution, as well as on the neutron scattering length density (NSLD) of lipids; and R_t is the radius of gyration along the normal to the bilayer. From the latter parameter, the bilayer thickness d_b can be determined using the following equation [21]:

$$d_b = \sqrt{12} R_t. \tag{3}$$

In the Kratky–Porod model, the shape of the theoretical scattering curve depends only on one parameter describing the membrane, i.e., radius of gyration R_t, and does not depend on the size of the vesicles, inhomogeneities within the bilayer, initial intensity, etc.

In the model of spherical vesicles, they can be represented as a sphere, the shell of which is formed by a phospholipid bilayer, and the intensity is determined as follows [22]:

$$I(q) = \frac{\alpha}{V_2}\left(\frac{3V_1(\rho_1 - \rho_2) j_1(qR_1)}{qR_1} + \frac{3V_2(\rho_2 - \rho_1) j_1(qR_2)}{qR_2}\right)^2 + B, \tag{4}$$

where α is the volume fraction of the vesicle shell; V_1 is the volume of the vesicle without taking into account the volume of the bilayer; V_2 is the volume of the vesicle together with the bilayer; ρ_1 is the NSLD of the medium; ρ_2 is the NSLD of the bilayer; R_1 is the radius of the inner part of the vesicle; R_2 is the total radius of the vesicle (including the thickness of the bilayer); and j_1 is the spherical Bessel function of the first order j_1, which is defined as

$$j_1(x) = \frac{\sin x - x\cos x}{x^2}. \tag{5}$$

The scattering intensity is normalized to the volume, in which the scale factor is equivalent to the volume fraction of the shell. In the inner part of the vesicle, the NSLD is the same as that in the solvent. It should be noted that both of these models are relatively simple, since they do not consider water molecules at the head of the phospholipids, i.e., the membrane−water interface is considered to be sharp. The relative simplicity of the models avoids artificial effects, which are often presented as artifacts of multiparameter models.

The experimentally obtained curves were analyzed using the SasView software package [23]. In the analysis, the theoretically calculated curves for ULVs were convoluted with the following lognormal size distribution function of vesicles:

$$f(R, R_m, \sigma) = \frac{1}{\sqrt{2\pi}} \frac{1}{R\sigma} \exp\left\{-\frac{1}{2}\left(\frac{\ln R - \mu}{\sigma}\right)^2\right\}, \tag{6}$$

where R_m is the median size value, $\mu = \ln R_m$, $\sigma = \frac{p}{R_m}$, and p is the deviation from the median value. At the same time, the mean size value is $R_{mean} = \exp(\mu + \sigma^2/2)$.

The effect of experimental uncertainties in the SANS curves on the obtained results was estimated using the covariance matrix approach. The resulting diagonal terms of the matrix, which represent the relative uncertainties of the fitted parameters, were multiplied by the normalized chi-square function to obtain the uncertainties of the parameters in absolute units.
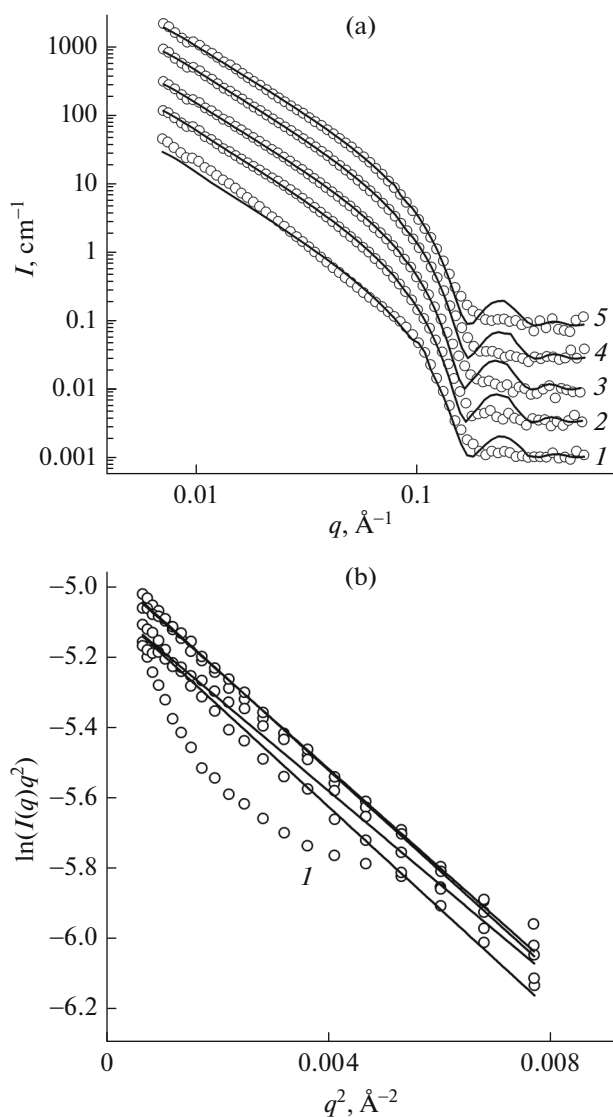
Fig. 1. (a) Small-angle neutron scattering curves obtained from the fluid phase of the DMPC samples at $T = 30°C$, which were extruded through filters with a pore diameter of 1000 Å and contained Ca^{2+} ions at concentrations of (*1*) 0, (*2*) 1, (*3*) 2, (*4*) 10, and (*5*) 30 mM; fitting was performed using the spherical vesicle model. (b) Kratky−Porod plot in coordinates $\ln(I(q)q^2)$ versus q^2 (*1*) at the same concentrations of Ca^{2+} ions.

RESULTS

In Figure 1a, the open circle points show the SANS curves for the fluid phase of DMPC phospholipids in a Ca^{2+} ion solution with concentrations of 0, 1, 2, 10, and 30 mM. The curves are analytically approximated using the Kratky−Porod approach and spherical vesicle model. It is the nonlinearity of the dependence plotted in $\ln(I(q)q^2)$ vs. q^2 coordinates (Fig. 1b) by using the Kratky−Porod approximation in the range of $q \in (0.02, 0.08)$ that makes it possible to determine the presence of multilamellar vesicles in the DMPC

sample without additives. This distortion is caused by the presence of a Bragg peak (broad and weakly pronounced) in the curve at $q = 0.08-0.1$ Å^{-1} (Fig. 1a). Multilamellar vesicles have a layer repeat distance of $d = 2\pi/q \approx 70$ Å.

The addition of a salt to the sample leads to complete destruction of the multilamellar vesicles, as evidenced by the disappearance of diffraction peaks in the curves corresponding to the remaining samples, as well as good linearity in the Kratky−Porod plot. Since the cations are bound to the phosphate group (dipole $P^- - N^+$), the charged bilayer is electrostatically repelled from the neighboring bilayer in the vesicle. The critical concentration of calcium ions, at which the destruction of all multilamellar vesicles in such a system occurs, was estimated as equal to 0.5 mM [24] and, consequently, our results confirm that the concentration of ions exceeded the critical value. It should also be noted that we obtained similar SANS curves for samples containing Mg^{2+} and Co^{2+} (Figs. 2 and 3).

The bilayer thickness d_b was determined using the two models mentioned above (i.e., the Kratky−Porod model and the model of spherical vesicles). Since the trends in the concentration dependences did not differ, we will further discuss only the results for the spherical vesicle model. The area per lipid A_L was calculated from the obtained d_b values by the formula $A_L = 2V_L/d_b$, where V_L is the volume occupied by one phospholipid molecule. According to the published data, V_L is 1101 Å^3 for DMPC at a temperature of 30°C [25] and $V_L = 1041$ Å^3 for DMPC in the gel phase at 20°C [26]. For DMPC without additives, the following parameters were obtained: in the fluid phase, $d_b = 36.2 \pm 0.7$ Å and $A_L = 60.8 \pm 0.7$ Å^2 when vesicles are extruded through filters with a pore diameter of 1000 Å, and $d_b = 36.1 \pm 0.4$ Å and $A_L = 61.0 \pm 0.4$ Å^2 when vesicles are extruded through filters with a pore diameter of 500 Å; in the gel phase, the corresponding parameters are $d_b = 37.8 \pm 0.7$ Å and $A_L = 55.1 \pm 0.7$ Å^2, and $d_b = 38.7 \pm 0.8$ Å and $A_L = 53.8 \pm 0.8$ Å^2, respectively. Hence, the obtained differences in the values of the thickness and area per lipid upon extrusion through filters with different pore diameters are insignificant, especially for lipid systems of DMPC in the fluid phase. Moreover, these results are in excellent agreement with the previously published results [27] for a membrane in DMPC vesicles without additives in the fluid phase ($T = 30°C$): $d_b = 36.3$ Å and $A_L = 60.6$ Å^2.

Figure 4 shows the dependences of the DMPC membrane thickness on the concentrations of Ca^{2+}, Mg^{2+}, and Co^{2+} for membranes in the fluid and gel phases. For Co^{2+}, the thickness variations are extremely weak. However, thickness variations are observed in the case of DMPC membranes with Ca^{2+} and Mg^{2+}. The bilayer thickness increases with an increase in the concentration of Ca^{2+} or Mg^{2+} ions in
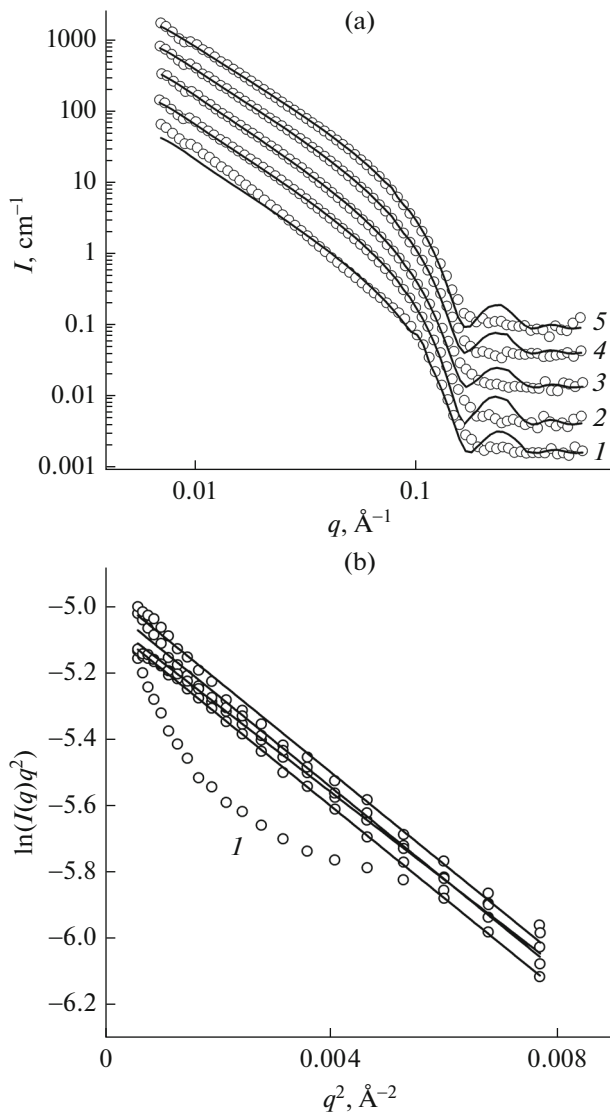
Fig. 2. (a) Small-angle neutron scattering curves obtained from the fluid phase of the DMPC samples at $T = 30°C$, which were extruded through filters with a pore diameter of 1000 Å and contained Mg^{2+} ions at concentrations of (*1*) 0, (*2*) 1, (*3*) 2, (*4*) 10, and (*5*) 30 mM; fitting was performed using the spherical vesicle model. (b) Kratky–Porod plot in coordinates $\ln(I(q)q^2)$ versus q^2 (*1*) at the same concentrations of Mg^{2+} ions.
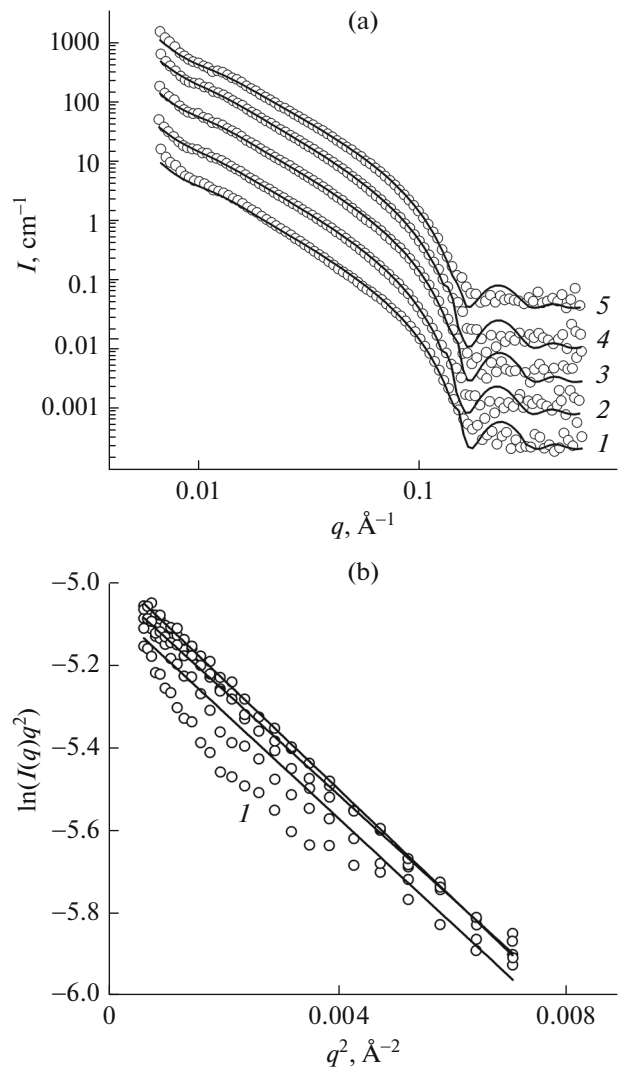
**Fig. 3.** Small-angle neutron scattering curves obtained from the fluid phase of the DMPC samples at $T = 30°C$, which were extruded through filters with a pore diameter of 500 Å and contained Co^{2+} ions at concentrations of (*1*) 0, (*2*) 1, (*3*) 2, (*4*) 10, and (*5*) 30 mM; fitting was performed using the spherical vesicle model. (b) Kratky–Porod plot in coordinates $\ln(I(q)q^2)$ versus q^2 (*1*) at the same concentrations of Co^{2+} ions.

the range of 0–1 mM, and then there is a slight tendency to a decrease in the membrane thickness in the fluid phase; in the gel phase, no decrease in the membrane thickness is observed in the case of Ca^{2+} ions, or there is a weak decrease in the case of Mg^{2+} ions. All changes in the membrane thickness in the fluid phase are characterized by relatively small differences (about 2 Å in the fluid phase versus about 3 Å in the gel phase).

In the fluid phase of membranes containing Ca^{2+} and Mg^{2+} ions, a sharp increase in the bilayer thickness is observed up to a maximum value of $d_b = 38.1 \pm$ 0.3 Å in the case of Ca^{2+} and $d_b = 38.0 \pm 0.3$ Å in the case of Mg^{2+}. When compared to DMPC without additives, the bilayer thickness increases by $\Delta d_b = 1.9 \pm$ 0.9 Å and $\Delta d_b = 1.8 \pm 1.0$ Å for Ca^{2+} and Mg^{2+}, respectively. Subsequently, the dependences show a tendency towards a decrease in the d_b value (by about 0.8 Å for DMPC + Ca^{2+} and 0.6 Å for DMPC + Mg^{2+}) in the ion concentration range of 1–30 mM. In the gel phase of DMPC, a sharp increase in the thickness from $d_b = 37.8 \pm 0.7$ Å to $d_b = 40.7 \pm 0.3$ Å occurs upon adding Ca^{2+} ions to DMPC in the concentration of 1 mM, which corresponds to a change in the thickness
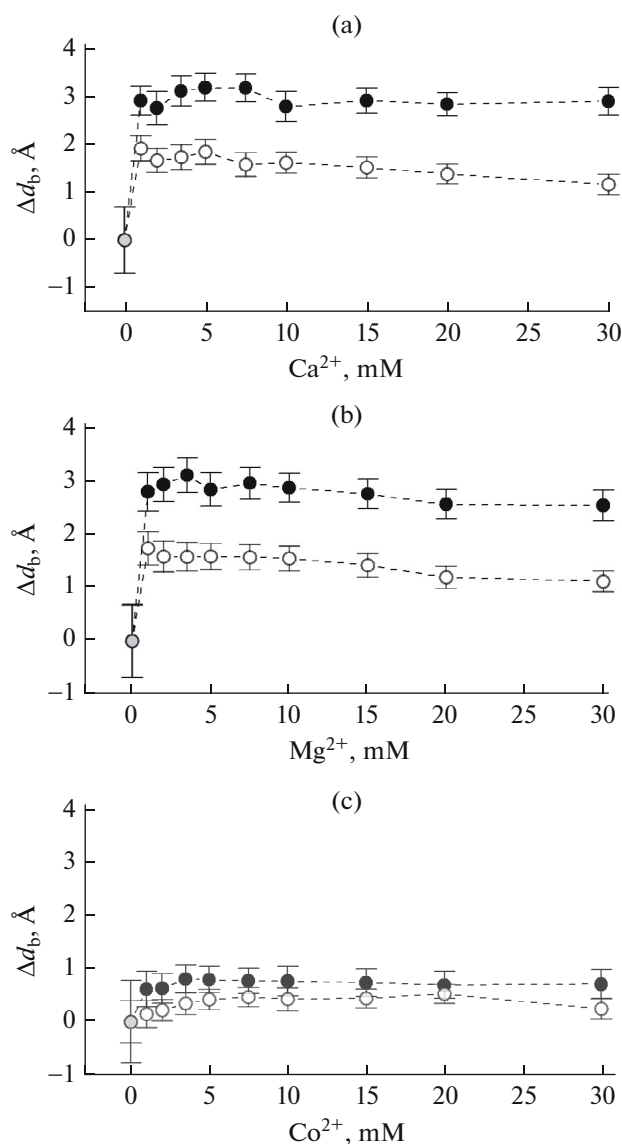
Fig. 4. Dependence of changes in the membrane thickness in the (○) fluid and (●) gel phases of the DMPC lipid systems on the concentrations of (a) Ca^{2+}, (b) Mg^{2+}, and (c) Co^{2+} ions.

by $\Delta d_b = 2.9 \pm 1.0$ Å. In the case of Mg^{2+}, a sharp increase in the thickness by $\Delta d_b = 2.8 \pm 1.1$ Å was also noted.

The change in A_L is inversely proportional to the change in d_b. Thus, the dependence of changes in the A_L values on the ion concentration is a mirror image of the analogous dependences for d_b. With the addition of salts in a concentration of 1 mM, A_L decreases by 3.0 ± 1.3 and 4.0 ± 1.0 Å^2 in the case of Ca^{2+}, and 2.8 ± 1.0 and 4.0 ± 1.1 Å^2 in the case of Mg^{2+} in the fluid and gel phases, respectively. Hence, the addition of salts (1 mM) results in a membrane that is more densely packed in comparison with the ion-free DMPC.

However, A_L either starts to increase (in the fluid phase) or barely changes (in the gel phase) with a further increase in the concentration of these cations.

DISCUSSION

According to numerous studies, the $P^- - N^+$ phospholipid dipole in a neutral medium is aligned along the tangent to the membrane surface and can freely rotate around the bilayer normal, as presented in [14, 28−30] and in Fig. 5a. In these works, except of [31−33], it was discussed that the increase in the membrane thickness can be explained by an electric field arising from the binding of ions with a negative charge to the phospholipid head, which orients the $P^- - N^+$ dipole along the bilayer normal. At the same time, it is well known that a change in the bilayer thickness (e.g., DPPC membrane thickness) occurs both in unilamellar vesicles and in oriented multilamellar membranes; in particular, the maximum membrane thickness (at Ca^{2+}-ion concentrations of around 2−3 mM) is detected by small-angle neutron scattering from ULVs, which is confirmed by neutron-diffraction experiments on oriented multilamellar membranes of the same DPPC + Ca^{2+} system [14, 28]. This allows us to assert changes in the membrane thickness particularly due to electrostatic interactions in the given concentration range and also to assume the presence of processes similar to those discussed in [24] only in the concentration range of 0−1 mM Ca^{2+} ions for our systems. Moreover, the substantial effect of surface curvature on the membrane thickness is excluded in the case of vesicles.

As established by computer simulation, Ca^{2+} and Mg^{2+} ions are localized at the phosphate and ether bonds of the carboxyl groups of DMPC [34]. In addition, the bound ions cause dehydration of the membrane, which leads to the formation of a denser phospholipid packing, as evidenced in our experiment by a decrease in the area per lipid molecule (in the Ca^{2+}-ion concentration range of 0−1 mM). Moreover, Ca^{2+} ions dehydrate the membrane more efficiently [35] than Mg^{2+} ions, whose strong hydrophilicity makes it difficult to bind to phospholipids [36].

As a result of binding of ions to the membrane, the electric field rearranges the phospholipid molecules in the membrane so that negatively charged phosphate groups of neighboring molecules are oriented toward positively charged phospholipids with the formation of ion bridges (Fig. 5b) [33]. Hence, quite strong Coulomb interaction in the resulting $PO_4^- - Me^{2+} - PO_4^-$ ion bridges leads to a decrease in the area per lipid and to a consequent increase in the thickness. In this case, the formation of ion bridges is a rather fast process that leads to the adsorption of ions from the solution on the membrane [37].

In our samples, a further increase in the concentration of ions in the solution leads, apparently, to saturation of the membrane structure changes. This can be explained by the lack of free sites for the formation of ion bridges. However, it is more likely that the influence of spatial restrictions plays a role here, which prevents further changes in the membrane structure, i.e., gives rise to the impossibility of its subsequent compression in the lateral direction. Nevertheless, the tendency toward a decrease in the membrane thickness with an increase in the concentration of ions in the membrane in the range of 1−30 mM may be caused by excessive lateral pressure in the hydrophobic region of the membrane, which leads to the inclination of phospholipid molecules relative to the normal of the bilayer (Fig. 5c). It should be noted that D. Huster et al. reported the effect of Ca^{2+} ions on hydrophobic chains of DMPC [31].

In the gel phase, the effect of a change in the structural parameters of the DMPC membrane in the range of 1−30 mM is weakly pronounced, since the membrane in the gel phase is more rigid than in the fluid phase. In addition, the self-diffusion coefficient of DMPC molecules in the fluid phase is an order of magnitude higher than the corresponding value of the gel phase [38]. Probably, this prevents the phospholipid molecules from tilting relative to the normal. According to the experimental results obtained for the membranes with Mg^{2+} ions, which are similar to the results with Ca^{2+} ions, the interactions of DMPC with Mg^{2+} can be described within the same model. Thus, we extend the above interaction model to our systems containing DMPC vesicles with Ca^{2+} and Mg^{2+} ions.

The described rearrangement of phospholipid molecules requires the presence of long-range electrostatic attraction between the phospholipid−ion complexes. The electrostatic effect of ions in a solution with a dielectric constant equal to the dielectric constant of the lipid head group in the lateral direction ($\varepsilon_r = 75$ [39]) is described by the Debye screening length, as follows [40]:

$$b = \sqrt{\frac{\varepsilon_0 \varepsilon_r kT}{e^2 \sum n_i z_i^2}}, \quad (7)$$

where ε_0 is the vacuum permittivity, n_i is the concentration of ions of the ith type, and z_i is the charge of ions of the ith type. With an increase in the ion concentration in the range from 1 to 30 mM, the Debye screening length b decreases from 55 to 10 Å. These values are an order of magnitude larger than the characteristic average distances between phospholipid molecules, which are approximately equal to $l = \sqrt{A_L} \approx 7.5$ Å. Thus, we suppose that due to the rearrangement of phospholipid molecules, the Debye screening length of the lipid system, which includes ions bound to phospholipid molecules, is below the l value for the
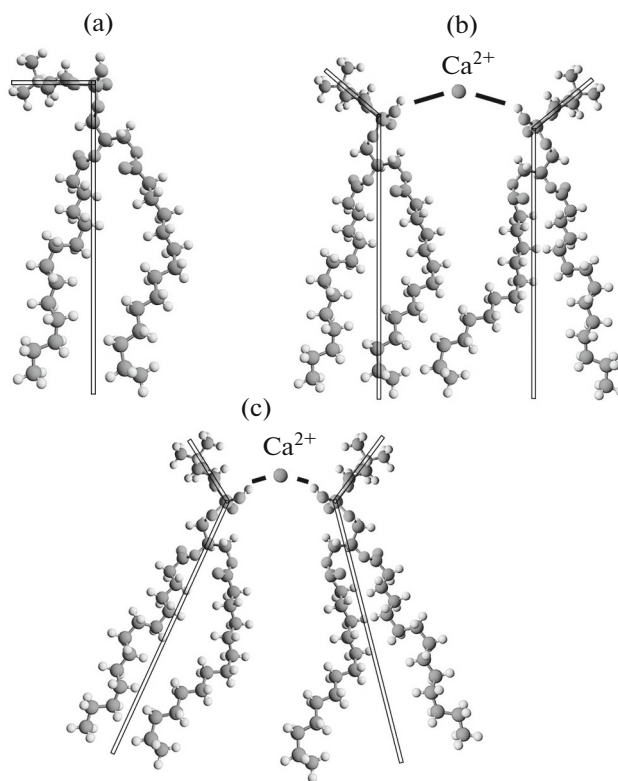
Fig. 5. Graphical interpretation of the changes in the thickness of the DMPC membrane: (a) a DMPC molecule (straight lines represent a coarse model of the molecule); (b) the formation of an ion bridge $PO_4^- - Ca^{2+} - PO_4^-$ by the electrostatic attraction of neighboring phospholipid molecules to the ion and, in addition, by changing the spatial orientation of the $P^- - N^+$ dipoles of phospholipids; (c) tilting of the phospholipid molecules relative to the normal of the bilayer.

entire investigated range of ion concentrations in a solution (i.e, $C < 30$ mM).

It should be noted that the Debye screening length also closely correlates with the charge density of the membrane, particularly, with the average distance between ions bound to phospholipids. The number of ions bound to the membrane can be estimated by the Langmuir adsorption isotherm, expressed as follows [14]:

$$\frac{X_b}{1 - nX_b} = K\left(C_{Ca^{2+}} - X_b C_l\right), \quad (8)$$

where X_b is the ratio of the number of bound ions to the total number of phospholipid molecules (mol/mol), n is the number of phospholipid molecules bound to one Ca^{2+} ion, $C_{Ca^{2+}}$ is the concentration of Ca^{2+} ions, and K is the binding constant. In [24], the binding constant of Ca^{2+} ions in DMPC vesicles in the fluid phase was estimated as close to 19 M^{-1}, which agrees with the results of another study related to DPPC membranes containing Ca^{2+} ions [41]. The n value is taken to be

equal to either 1 or 2, which corresponds to the binding of an ion with one or two phospholipid molecules, respectively [41, 42]. In the Ca^{2+} ion concentration range of $1-30$ mM, the results of calculating the X_b values for different n do not differ substantially and are about 15 ions per 1000 molecules of phospholipid DMPC at 1 mM (324 ions per 1000 phospholipid molecules at 30 mM). A similar value was obtained in [43] for the DPPC + Na^+ systems at 1 mM ($22-24$ ions per 1000 DPPC molecules). Thus, the average distance between ions—on the condition that they are uniformly distributed over the membrane surface—is 62 Å at 1 mM (13.5 Å at 30 mM), which exceeds the calculated Debye screening lengths over the entire studied concentration range. This confirms the lack of interactions between cations, which would potentially lead to their repulsion.

Co^{2+} ions have little effect on the structural parameters of the DMPC membrane. Hence, the electrostatic interactions of Co^{2+} in the bilayer, which are included in the model of the interaction of Ca^{2+} and Mg^{2+} ions with DMPC phospholipid molecules, are somewhat different and weakly pronounced in comparison with the interactions of Ca^{2+} and Mg^{2+}. This can directly relate to the different physical properties of these ions and can also be explained by different levels of hydration, strength, and places of binding of ions with head groups of phospholipids. For example, the binding constants of Ca^{2+} and Mg^{2+} with egg lecithin were determined in [4] as equal to $K = 40$ M^{-1} for Ca^{2+} and $K = 30$ M^{-1} for Mg^{2+}. This indicates the strong binding of these cations in comparison with Co^{2+}, which binds relatively weakly ($K = 1.2$ M^{-1} at 10 mM) [44] and barely has an effect on the membrane rigidity and the size of the DMPC vesicles [45].

In addition, it is important to take into consideration the ion sizes, since smaller ion sizes are capable of creating strong electric fields, which leads to higher values of the hydration energy [46]. For example, Ca^{2+} has an ionic radius of 1.00 Å, while the radius of Mg^{2+} ions is only 0.72 Å [33, 47]. Co^{2+} has an ionic radius close to that of Mg^{2+}, namely, 0.75 Å [48]. As it was shown in [28], the different effect of divalent metal ions on the thickness of phospholipid membranes is also associated with the individual behavior of the ions during their hydration. In our case, it is known that Co^{2+} has six molecules in the first hydration shell. At the same time, water molecules near Mg^{2+} ions (six to seven molecules) and Ca^{2+} ions (six to eight molecules) are arranged in a similar way [33, 47, 49]. Moreover, the electric field of these ions extends beyond the first hydration shell and polarizes water molecules in the second shell, thereby modifying the network of hydrogen bonds. Therefore, the arrangement of water molecules for these cations in the second hydration shell is determined by various methods as follows [47–

49]: from one to six water molecules for Ca^{2+}, 7 (12) for Mg^{2+}, and 5.7 (9.6) for Co^{2+}.

It follows from the above that Co^{2+} cations do not fundamentally differ in physical properties during hydration, for example, from Mg^{2+} ions, and occupy some intermediate position between Mg^{2+} and Ca^{2+} in accordance with their parameters. However, at the same time, it is important that cobalt is a transition metal that has seven d electrons in the outer shell. In this regard, the Co^{2+} ion in aqueous solutions forms high-spin complexes with an ordered octahedral arrangement of water molecules in the first hydration shell [50, 51]. This probably causes the splitting of degenerate electronic states and the appearance of new states with not only higher energies, but also with lower energies that give rise to an increase in the stability of the ion in the field of water molecules, which may prevent Co^{2+} ions from binding to the head of phospholipid molecules, in particular, to negatively charged PO_4 and CO_2 groups that have vacant high-energy orbitals [18]. This peculiarity of binding closely correlates with the localization of ions in the membrane near individual atomic groups of the phospholipid head, which also largely depends on the concentration of ions in a solution.

It should be finally noted that such a consideration of the interactions of ions with water molecules, as well as the experimental results obtained in this study, clearly elucidate the different binding specificity and localization of Ca^{2+}, Mg^{2+}, and Co^{2+} ions in the head groups of DMPC phospholipids. It should be emphasized that differences in the localization of ions and changes in the membrane thickness caused by them can—together or separately—affect the conformations and functions of various membrane proteins and peptides possessing charges.

CONCLUSIONS

Using small-angle neutron scattering, it is shown that Ca^{2+} and Mg^{2+} cations cause similar structural changes in DMPC membranes through conformational changes in the head groups and the formation of ion bridges over the entire range of the studied ion concentrations. In the concentration range of $1-30$ mM, phospholipid molecules are rearranged in the membrane with a tilt of the hydrophobic tails. However, all these changes are extremely weak in the case of Co^{2+} cations, which can be explained by the fact that the binding sites of Co^{2+} are different from Ca^{2+} and Mg^{2+}. It is also shown that the electrostatic interaction model previously developed for the DPPC (DMPC) + Ca^{2+} systems can be extended to the DMPC + Mg^{2+} systems.

It is established that the structural changes in the membrane, which are induced by Ca^{2+} and Mg^{2+} cations, also depend on the thermodynamic phase of the

DMPC lipid systems. In the gel phase, there are pronounced conformational changes in the head groups of phospholipids (the change in the membrane thickness is 1/3 greater than that in the fluid phase). On the other hand, a decrease in the membrane thickness associated with the tilt of phospholipid molecules in the bilayer with ions in the concentration range of 1–30 mM is less pronounced in the gel phase compared to the fluid phase.

FUNDING

REFERENCES

1. G. Pabst, N. Kučerka, M.-P. Nieh, M. C. Rheinstädter, and J. Katsaras, Chem. Phys. Lipids **163**, 460 (2010).
https://doi.org/10.1016/j.chemphyslip.2010.03.010

2. B. Alberts, A. Johnson, J. Lewis, D. Morgan, M. Raff, K. Roberts, and P. Walter, *Molecular Biology of the Cell* (Garland Science, New York, 2015).

3. P. Lo Nostro and B. W. Ninham, Chem. Rev. **112**, 2286 (2012).
https://doi.org/10.1021/cr200271j

4. S. A. Tatulian, Eur. J. Biochem. **170**, 413 (1987).
https://doi.org/10.1111/j.1432-1033.1987.tb13715.x

5. N. Kučerka, E. Papp-Szabo, M.-P. Nieh, T. A. Harroun, S. R. Schooling, J. Pencer, E. A. Nicholson, T. J. Beveridge, and J. Katsaras, J. Phys. Chem. B **112**, 8057 (2008).
https://doi.org/10.1021/jp8027963

6. J. A. Beto, Clin. Nutr. Res. **4**, 1 (2015).
https://doi.org/10.7762/cnr.2015.4.1.1

7. U. Gröber, J. Schmidt, and K. Kisters, Nutrients **7**, 8199 (2015).
https://doi.org/10.3390/nu7095388

8. G. Bánfalvi, Heavy metals, trace elements and their cellular effects, in *Cellular Effects of Heavy Metals*, Ed. by G. Bánfalvi (Springer, Amsterdam, Netherlands, 2011), p. 3.
https://doi.org/10.1007/978-94-007-0428-2_1

9. H. I. Petrache, T. Zemb, L. Belloni, and V. A. Parsegian, Proc. Natl. Acad. Sci. U. S. A. **103**, 7982 (2006).
https://doi.org/10.1073/pnas.0509967103

10. L. J. Lis, W. T. Lis, V. A. Parsegian, and R. P. Rand, Biochemistry **20**, 1771 (1981).
https://doi.org/10.1021/bi00510a010

11. C. G. Sinn, M. Antonietti, and R. Dimova, Colloids Surf., A **282**, 410 (2006).
https://doi.org/10.1016/j.colsurfa.2005.10.014

12. A. Lee, Biochim. Biophys. Acta **1666**, 62 (2004).
https://doi.org/10.1016/j.bbamem.2004.05.012

13. N. Kučerka, M.-P. Nieh, J. Pencer, J. N. Sachs, and J. Katsaras, Gen. Physiol. Biophys. **28**, 117 (2009).
https://doi.org/10.4149/gpb_2009_02_117

14. D. Uhríková, N. Kučerka, J. Teixeira, V. Gordeliy, and P. Balgavý, Chem. Phys. Lipids **155**, 80 (2008).
https://doi.org/10.1016/j.chemphyslip.2008.07.010

15. N. Kučerka, J. Pencer, J. N. Sachs, J. F. Nagle, and J. Katsaras, Langmuir **23**, 1292 (2007).
https://doi.org/10.1021/la062455t

16. A. I. Kuklin, D. V. Soloviev, A. V. Rogachev, P. K. Utrobin, Y. S. Kovalev, M. Balasoiu, O. I. Ivankov, A. P. Sirotin, T. N. Murugova, T. B. Petukhova, Y. E. Gorshkova, R. V. Erhan, S. A. Kutuzov, A. G. Soloviev, and V. I. Gordelii, J. Phys.: Conf. Ser. **291**, 7 (2011).
https://doi.org/10.1088/1742-6596/291/1/012013

17. A. I. Kuklin, A. D. Rogov, Y. E. Gorshkova, P. K. Utrobin, Y. S. Kovalev, A. V. Rogachev, O. I. Ivankov, S. A. Kutuzov, D. V. Soloviov, and V. I. Gordeliy, Phys. Part. Nucl. Lett. **8**, 119 (2011).
https://doi.org/10.1134/S1547477111020075

18. A. G. Soloviev, T. M. Solovjeva, O. I. Ivankov, D. V. Soloviov, A. V. Rogachev, and A. I. Kuklin, J. Phys.: Conf. Ser. **848**, 7 (2017).
https://doi.org/10.1088/1742-6596/848/1/012020

19. L. A. Feigin and D. I. Svergun, *Structure Analysis by Small-Angle X-Ray and Neutron Scattering* (Springer, New York, 1987).
https://doi.org/10.1007/978-1-4757-6624-0

20. M. A. Kiselev, D. Lombarde, A. M. Kiselev, P. Lezi, and V. L. Aksenov, Poverkhn.: Rentgenovskie, Sinkhrotronnye Neitr. Issled., No. 11, 24 (2003).

21. N. Kučerka, M. A. Kiselev, and P. Balgavý, Eur. Biophys. J. **33**, 328 (2004).
https://doi.org/10.1007/s00249-003-0349-0

22. G. Fournet, *Small-Angle Scattering of X-Rays* (Wiley, New York, 1955).

23. SasView (2020). Sas View for Small Angle Scattering Analysis. https://www.sasview.org/. Cited May 25, 2020.

24. Yu. E. Gorshkova, PhD. Dissertation in Mathematics and Physics (Joint Inst. Nucl. Res., Dubna, 2017).

25. J. F. Nagle and S. Tristram-Nagle, Biochim. Biophys. Acta **1469**, 159 (2000).
https://doi.org/10.1016/S0304-4157(00)00016-2

26. J. F. Nagle and D. A. Wilkinson, Biophys. J. **23**, 159 (1978).
https://doi.org/10.1016/S0006-3495(78)85441-1

27. N. Kučerka, S. Tristram-Nagle, and J. F. Nagle, J. Membr. Biol. **208**, 193 (2005).
https://doi.org/10.1007/s00232-005-7006-8

28. N. Kučerka, E. Dushanov, K. T. Kholmurodov, J. Katsaras, and D. Uhríková, Langmuir **33**, 3134 (2017).
https://doi.org/10.1021/acs.langmuir.6b03228

29. J. Seelig, Cell Biol. Int. Rep. **14**, 353 (1990).
https://doi.org/10.1016/0309-1651(90)91204-H

30. Y. Izumitani, J. Colloid Interface Sci. **166**, 143 (1994).
https://doi.org/10.1006/jcis.1994.1281

31. D. Huster, G. Paasche, U. Dietrich, O. Zschörnig, T. Gutberlet, K. Gawrisch, and K. Arnold, Biophys. J. **77**, 879 (1999).
https://doi.org/10.1016/S0006-3495(99)76939-0

32. R. Zidovetzki, A. W. Atiya, and H. De Boeck, Membr. Biochem. **8**, 177 (1989).
https://doi.org/10.3109/09687688909025830

33. H. Binder and O. Zschörnig, Chem. Phys. Lipids **115**, 39 (2002).
https://doi.org/10.1016/S0009-3084(02)00005-1

34. C. T. M. Le, A. Houri, N. Balage, B. J. Smith, and A. Mechler, Front. Mater. **5**, 1 (2019).
https://doi.org/10.3389/fmats.2018.00080

35. S. De Kanti, N. Kanwa, V. Ahamed, and A. Chakraborty, Phys. Chem. Chem. Phys. **20**, 14796 (2018).
https://doi.org/10.1039/c8cp01774c

36. J. Yang, C. Calero, M. Bonomi, and J. Marti, J. Chem. Theory Comput. **11**, 4495 (2015).
https://doi.org/10.1021/acs.jctc.5b00540

37. M. Javanainen, A. Melcrová, A. Magarkar, Z. P. Jurkiewic, M. Hof, P. Jungwirth, and H. Martinez-Seara, Chem. Commun. **53**, 5380 (2017).
https://doi.org/10.1039/c7cc02208e

38. C. Scomparin, S. Lecuyer, M. Ferreira, T. Charitat, and B. Tinland, Eur. Phys. J. E **28**, 211 (2009).
https://doi.org/10.1140/epje/i2008-10407-3

39. H. A. Stern and S. E. Feller, J. Chem. Phys. **118**, 3401 (2003).
https://doi.org/10.1063/1.1537244

40. J. M. Moore, *Physical Chemistry*, 4th ed. (Prentice-Hall, Englewood Cliffs, NJ, 1972).

41. K. Satoh, Biochim. Biophys. Acta **1239**, 239 (1995).
https://doi.org/10.1016/0005-2736(95)00154-U

42. C. Altenbach and J. Seelig, Biochemistry **23**, 3913 (1984).
https://doi.org/10.1021/bi00312a019

43. E. Chibowski and A. Szcześ, Adsorption **22**, 755 (2016).
https://doi.org/10.1007/s10450-016-9767-z

44. A. McLaughlin, C. Grathwohl, and S. McLaughlin, Biochim. Biophys. Acta **513**, 338 (1978).
https://doi.org/10.1016/0005-2736(78)90203-1

45. J. Umbsaar, E. Kerek, and E. J. Prenner, Chem. Phys. Lipids **210**, 28 (2018).
https://doi.org/10.1016/j.chemphyslip.2017.11.016

46. E. Eriksson, *Principles and Applications of Hydrochemistry* (Springer, Amsterdam, 1985).
https://doi.org/10.1007/978-94-009-4836-5

47. F. David, V. Vokhmin, and G. Ionova, J. Mol. Liq. **90**, 45 (2001).
https://doi.org/10.1016/S0167-7322(01)00106-4

48. Y. Marcus, J. Chem. Soc., Faraday Trans. **87**, 2995 (1991).
https://doi.org/10.1039/FT9918702995

49. H. Ohtaki and T. Radnai, Chem. Rev. **93**, 1157 (1993).
https://doi.org/10.1021/cr00019a014

50. H. Ohtaki and H. Yamatera, *Structure and Dynamics of Solutions* (Elsevier, Oxford, 1992).

51. I. Bertini, C. Luchinat, G. Parigi, and E. Ravera, *NMR of Paramagnetic Molecules: Applications to Metallobiomolecules and Models*, 2nd ed. (Elsevier, Amsterdam, 2016).

52. R. Crichton, *Biological Inorganic Chemistry: A New Introduction to Molecular Structure and Function*, 3rd ed. (Elsevier, Amsterdam, 2018).

Translated by O. Kadkin